PROCESSING SPACE FENCE RADAR CROSS-SECTION DATA TO PRODUCE SIZE AND MASS ESTIMATES

Luis Baars[*] and Doyle Hall[†]

With the addition of the Space Fence (SFK) radar to the Space Surveillance Network (SSN), the NASA Conjunction Assessment Risk Analysis (CARA) team now has access to radar cross-section (RCS) measurements for many Earth orbiting satellites. The CARA team has developed a process to estimate satellite sizes and masses from the SFK RCS measurement data. This study describes the processes used to filter the RCS data, defines the algorithms used to estimate satellite sizes and masses, and presents comparisons of estimated values against known satellite sizes and masses.

INTRODUCTION

The NASA Conjunction Assessment Risk Analysis (CARA) team provides satellite close approach analysis for all non-crewed NASA Earth-orbiting satellites for collision avoidance and space environment protection. The team computes the probability of collision (P_c) as one of the key metrics that are assessed in analyzing the risk in order to recommend the correct mitigative actions required. The CARA processing system first detects candidate close encounters in various orbital regimes involving high value assets up to ten days in advance using a screening-volume approach, based on the latest available satellite tracking data and orbit determination (OD) state and covariance solutions.[1,2]

For each conjunction, CARA assesses the collision risk using a set of established semi-analytical, and Monte Carlo P_c approximation methods.[3,4,5,6] A key component of each P_c calculation is an estimate of the combined hard-body radius (HBR) of the two objects involved in the conjunction. In CARA operations, the combined HBR is composed of the known hard-body protection radius of the NASA satellite, often referred to as the "primary", and a default HBR of 1.5 meters for the other object involved in the conjunction, the "secondary".

When using such a default value for the secondary, the estimated P_c could be overestimated or underestimated if the actual secondary HBR is significantly different from 1.5 meters. In a CARA technical analysis from 2014, this default HBR was selected because it encompasses 98% of the debris objects likely to be encountered in the Low-Earth Orbit (LEO) and Highly-Eccentric Orbit (HEO) orbital regimes.[7] This is a fairly conservative HBR to apply to all objects since the analysis also indicates that ~85% of LEO/HEO debris objects have a characteristic size (e.g., diameter) of 20 cm or less, which translates to an HBR of 10 cm or less.[7] While choosing such a conservative secondary HBR value reduces the risk of potentially missing a high interest event, it

[*] Conjunction Assessment Research Analyst, Omitron Inc., 555 E. Pikes Peak Ave, #205, Colorado Springs, CO 80903. luis.baars@omitron.com

[†] Senior Conjunction Assessment Research Scientist, Omitron Inc., 555 E. Pikes Peak Ave, #205, Colorado Springs, CO 80903. doyle.hall@omitorn.com

also increases the computational load on automated processing systems. The introduction of large constellations such as Starlink and OneWeb, and the proliferation of debris from antisatellite tests increase the likelihood of close approach events occurring, which increases the computational load even further.[8,9]

The conversion from a radar cross-section (RCS) measurement to an object size estimate uses the NASA Size Estimation Model (SEM).[10] The intended use for the NASA SEM is to produce size estimates of fragmentation debris 20 cm or smaller based on an entire distribution of RCS measurements.[7] Historically, the RCS data available to the CARA team consisted of averages of RCS values for each sensor and object pair. Using such average RCS values with the NASA SEM model could potentially introduce inaccurate results since averaged values would not be in alignment with the developmental principles of the model. This is a contributing factor as to why the CARA team has not previously used RCS data to estimate object sizes.

The Space Fence (SFK) radar provides multiple RCS measurements for each observed object, each of which are used to generate a size estimate using the NASA SEM. The analysis uses the resulting distribution of sizes (which is typically widely scattered) to approximate the size-estimation uncertainty probability density function (PDF) for each object. However, before the RCS data can be used for this purpose, several filtering processes must be performed in order to remove time periods when the SFK sensor does not meet RCS calibration expectations needed for accurately estimating the size of the observed object. The initial filter eliminates days when SFK RCS measurements do not meet these expectations, and the remaining RCS data for each object are examined using analysis of variance (ANOVA) techniques. In the CARA implementation, the ANOVA process identifies time periods when SFK is not providing RCS data consistent with historical expectations. The process runs iteratively until it finds a consistent subset of RCS data, or no data remains. The remaining RCS data provide a distribution used to estimate the size and mass of each object. Calculating mass estimates entails combining the HBR estimates and ballistic coefficient (BC) values.

The primary goal of this analysis is to provide a more realistic assessment of collision risk for conjunctions involving objects with unknown or unpublished dimensions, by accounting for the magnitude and uncertainty of RCS-based satellite size and mass estimates. Specifically, accounting for the HBR uncertainty distribution of unknown secondary satellites provides more accurate estimates of conjunction P_c values — especially compared to the current method of simply using a default HBR value of 1.5 m for all unknown objects. This allows CARA to better identify high-risk events in Earth's increasingly congested space environment. RCS-based mass estimates provide the means to evaluate the consequences of potential collisions, by determining if they may be catastrophic (in which both objects are completely shattered), and also by estimating the expected number of fragments. In summary, this paper focuses on four specific aspects of RCS-based conjunction risk assessment:

1) Data filtering techniques, which provide an RCS data set appropriate for estimating the sizes and masses of unknown objects.
2) Estimating the resulting object size uncertainty distributions, as well as calibrated estimates of statistically expected HBR values and associated variances.
3) Estimating collision probabilities for conjunctions involving unknown objects, using a method that accounts for the magnitude and uncertainty of the RCS-based HBR estimates.
4) Estimating unknown object masses by combining object BC distributions with the RCS-based HBR distributions, which allows the evaluation of the catastrophic nature and fragment production of any potential collisions.

RADAR CROSS SECTION MEASUREMENT DATA

The SFK radar began trial operations on November 25, 2019 and became operational on March 28, 2020.[11,12] The Space Fence radar receives and processes both the principal and orthogonal polarizations of the returned energy from radar returns. These radar cross-section measurements for both polarizations are provided with each SFK observation, and this marks the first-time observation-level RCS measurements are regularly provided by a sensor on the SSN. Prior to this development, sensors provided weekly summaries of RCS values received for each object. However, without full knowledge of the methods used to create the RCS summary data, the CARA team was hesitant in using these weekly summary data for HBR estimation.

Since the beginning of the SFK trial operations period, the CARA team has collected observation-level SFK RCS measurement data for the purpose of HBR estimation. As of May 1st, 2022, the dataset consists of over forty-five million observations across more than 25,000 unique objects, for an average of ~1,700 observations per object.

THE NASA RCS-BASED SIZE ESTIMATION MODEL

The NASA size estimation model (SEM) provides a semi-empirical method to convert RCS measurements for an unknown satellite into a statistical ensemble of estimates for the "characteristic length" of the object.[13,14] The characteristic length is not equivalent to the hard-body radius, but instead represents the average of the largest dimensions of an object measured along three orthogonal axes, which corresponds to the diameter for spherical objects.[13,14] Applying the SEM to the nth RCS measurement available for the jth satellite yields

$$D_{j,n} = \begin{cases} \lambda_{j,n} \sqrt{4z/\pi} & z > 5 \\ \lambda_{j,n} \sqrt[6]{4z/(9\pi^5)} & z < 0.03 \\ \lambda_{j,n} g_{SEM}(z) & otherwise \end{cases} \tag{1}$$

with $D_{j,n}$ denoting the characteristic length (m) corresponding to the RCS measurement[*], $\lambda_{j,n}$ the radar wavelength (m), and $z = Y_{j,n}/\lambda_{j,n}^2$, with $Y_{j,n}$ representing the measured RCS value (m²). Stokely et al provide an interpolation table for the function $g_{SEM}(z)$.[13,14]

RCS UNITS AND CONVERSIONS

The CARA processing system receives RCS measurements in units of square meters (m²). Unless explicitly specified otherwise, the RCS comparisons and calculations used within this document are expressed in decibels relative to one square meter (dBsm). The conversion between m² and dBsm is

$$RCS_{dBsm} = 10 * \log_{10}(RCS_{m^2}) \tag{2}$$

RCS DATA FILTERING

Numerous error sources can introduce both randomness and bias into RCS measurements.[10] Major contributing sources of error can include radar calibration uncertainties, propagation uncertainties, and signal processing effects, among others.[10] Several data filtering techniques have

---

[*] Reference the Notation section for a full list of mathematical notations used within this paper.

been implemented in order to remove RCS measurement data of a level of quality not appropriate for object size estimation.

Calibration Sphere Filtering

When processing raw RCS data from the Eglin FPS-85 radar, Hejduk and DePalma noted that occasional calibration problems occurred despite the nominal calibration procedures regularly followed by the site.[15] In order to maintain a well-calibrated dataset, Hejduk and DePalma included data only for time periods when all RCS measurements for a set of calibration satellites remained within 1.5 dBsm of their known reference values.[15] A similar approach has been implemented for CARA using three calibration satellites with catalog object IDs of 900, 902, and 2826. Table 1 lists the diameter for each calibration sphere used.

Table 1. Calibration Sphere Characteristics

Object ID	Diameter (m)
900	0.3556
902	0.3556
2826	0.508

For each calibration sphere, all RCS measurements are split into bins based on the day when the measurement was collected. For each day, all RCS measurements are examined and if any one measurement is more than 1.5 dBsm from the reference RCS, then the day is marked as a day from which data for size estimation purposes will not be employed. The overall designation of such days is the union of all such designated days from the results from examining all three calibration satellites. All RCS measurements collected on these days that are not appropriate for size estimation are ignored in subsequent processing.

ANOVA Filtering

Once calibration sphere filtering is complete, the RCS measurement data set has been reduced down to a set of measurements collected when the SFK sensor's data meet standards for size estimation. However, in order to account for other error sources that introduce randomness and bias, CARA needs a way to identify and remove inconsistent RCS measurements without a priori knowledge of an object's size or shape. In the case of irregularly shaped tumbling debris, it is expected that a wide range of RCS measurements could be received; therefore, the ultimate goal would not be to necessarily remove the randomness, but instead to remove relative biases.

The analysis assumes that the sizes and radar reflection properties of typical orbital objects do not change significantly over time, so the long-term average distribution of RCS measurements also remains unchanged. By dividing the RCS measurements into monthly bins, CARA has used analysis of variance (ANOVA) techniques to compare the monthly means over time. ANOVA is a generalized version of the Student's *t*-test used to compare the means of three or more groups.[16] In ANOVA, the alternative hypothesis assumes that a statistically significant difference exists between the means of the groups compared, while the null hypothesis assumes no statistically significant difference between the means.[16,17] There are many different flavors of ANOVA used for different experimental designs, including one-way ANOVA, two-way ANOVA, and nested ANOVA.[17] CARA's implementation only uses one-way ANOVA and its derivatives. The goal of the ANOVA testing is to identify statistically discrepant data (i.e., outliers), which represent

spurious instrumental or environmental effects rather than properties of the observed object. Eliminating these outliers produces a subset of RCS measurements that are consistent over time, and appropriate for use in object size and mass estimation.

In order to apply basic one-way ANOVA to a problem, three assumptions should be met: 1) the observations are statistically independent, 2) the observations are normally distributed, and 3) the data are homoscedastic (i.e. the data have the same standard deviation in different groups).[17] While the first assumption is the hardest to prove conclusively, CARA has made the assumption that the RCS measurements are independent because they are the products of different tracking sessions and therefore should not share systematic errors that do not manifest themselves as discernable biases. Nominally, if the observation data are not normally distributed the Kruskal-Wallis test is used instead of one-way ANOVA.[17] McDonald recommends the use of one-way ANOVA regardless of the normality of the observations.[17] For simplicity, CARA has chosen to use one-way ANOVA whether or not the observation data are normally distributed. If the data are not homoscedastic, the recommendation is to use Welch ANOVA instead of one-way ANOVA.[17] Further details on ANOVA will be provided below.
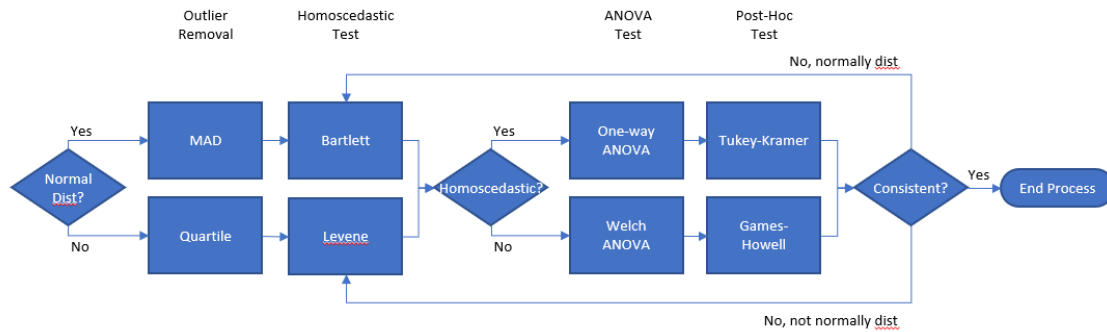

Figure 1. ANOVA Processing Workflow

Figure 1 depicts a high-level overview of the logic flow used by CARA's ANOVA RCS filter processing implementation. Use the figure as a reference to the processing steps outlined in the paragraphs below.

Normality Decision Point. At the very beginning of the process a Kolmogorov-Smirnov (K-S) test is performed to test whether or not the RCS data in each monthly group is normally distributed.[18] If all monthly groups are normally distributed, then the process flow follows the upper path for outlier removal and homoscedastic testing in Figure 1. Otherwise, the lower path is followed.

Outlier Removal. When all monthly groups are normally distributed, outlier identification and removal are performed using the scaled median of the absolute deviations about the median (MAD) method.[19,20] Otherwise, outliers are removed whenever measurements are more than 1.5 interquartile ranges above the upper quartile or below the lower quartile.[19,20] Regardless of the method used, outliers are identified and removed from individual monthly groups and not from the overall RCS distribution.

Homoscedastic Tests. After outlier removal occurs, the remaining data is tested for homoscedasticity, also known as the homogeneity of variances. Two tests can be employed to test for the homogeneity of variances; if all groups are normally distributed then Bartlett's test can be

used, otherwise Levene's test is recommended.[18,21,22] The results of this testing will determine which ANOVA and Post-Hoc tests can be used.

ANOVA Tests. The purpose of ANOVA is to test if the means of the measurement variable are the same for multiple groups.[17] In one-way ANOVA there is one dependent variable (i.e. the measurement variable) and one independent variable.[17] For CARA processing, the dependent variable is the RCS value and the independent variable is time (i.e., the month when the RCS measurement was collected), thus making one-way ANOVA an appropriate test for this experiment. The null hypothesis is that the means of the RCS measurements across all months are the same while the alternative hypothesis is that mean RCS of at least one month is different from the rest of the months. McDonald asserts that one-way ANOVA is not particularly sensitive to deviations from the normality assumption and recommends the use of one-way ANOVA over the Kruskal-Wallis test when the normality assumption is violated.[17] On the other hand, one-way ANOVA is sensitive to the heterogeneity of variances, especially when the number of observations in each group are dissimilar.[17] In these situations, McDonald recommends the use of Welch's ANOVA.[17] Both ANOVA tests generate a *p-value* to indicate if the null hypothesis is rejected. This *p-value* is used to determine if the RCS values are considered consistent or if a monthly group of measurements should be rejected as inconsistent measurements.

Post-Hoc Tests. The *p-value* generated by the ANOVA techniques simply provides an indicator that at least one group of data has a mean that is different from the rest of the groups. It does not identify which group is considered the most different from the rest of the groups. Tukey's Honestly Significant Different (HSD) test compares differences among sample means for significance.[23] Tukey's HSD test performs a pairwise comparison between all of the groups included in the ANOVA test. A separate *p-value* is provided for each possible pairwise combination of the groups, indicating how alike the means are to each other. In order to identify the group which is most unalike from the others, CARA sums the *p-values* for each individual group against all the other groups. The group with the lowest summed set of *p-values* is considered the most different from the other groups and is flagged as the group which will be eliminated.

For example, assume that five groups labeled A through E are examined using Tukey's HSD test that generates the *p-values* listed in Table 2. The summed *p-values* for each group would be: A = 2.0399, B = 1.9119, C = 0.8131, D = 2.0784, and E = 1.0721. In this example, group C would be identified as the most discrepant, and flagged for elimination.

Table 2. Sample *p-values* for a Hypothetical Tukey's HSD Test

	A	B	C	D	E
A	N/A	0.8935	0.0057	0.9960	0.1447
B	0.8935	N/A	0.0009	0.9858	0.0317
C	0.0057	0.0009	N/A	0.0037	0.8028
D	0.9960	0.9858	0.0037	N/A	0.0929
E	0.1447	0.0317	0.8028	0.0929	N/A

Much like the ANOVA testing, a separate post-hoc test is used when the variances are heterogeneous. Ruxton and Beauchamp recommend the use of the Games-Howell post-hoc test in

this situation.[24,25] Other than accounting for the heterogeneity of variances, CARA's use of the Games-Howell test to identify the most unlike group is exactly the same as Tukey's HSD test.

Consistency Decision Point. The final portion of the ANOVA filtering process determines whether or not the RCS data that has been examined is evaluated to be self-consistent. Recall that the null hypothesis from the ANOVA test is that the means of the monthly RCS data are the same. When the null hypothesis is rejected, the RCS data are deemed inconsistent, the month flagged as the most discrepant in the post-hoc testing is eliminated, and the filtering process loops back to the homoscedastic testing step using the remaining RCS data. The overall filtering process continues until the entire remaining RCS data set is evaluated to be consistent (i.e. the null hypothesis from the ANOVA test is accepted), only two months of data remain, or less than twenty RCS measurements remain. In the latter two cases, the ANOVA filtering process is considered inconclusive and all of the RCS data is flagged as inconsistent.

Testing indicates that the filtering process can be too aggressive when the ANOVA test threshold is set to the typical *p-value* of 0.05. As a result, the analysis reduces the *p-value* threshold to 0.01 in order to retain a larger fraction of RCS measurements.

Sample Filtering Results

Figure 2 and Figure 3 show a set of RCS measurements before and after ANOVA filtering for a piece of COSMOS 2251 debris generated by the collision with the Iridium 33 satellite in February 2009. The top subplot in each graph shows the raw RCS measurements. The color coding indicates if the measurement was accepted (blue) or eliminated for any one of various reasons: calibration sphere bad date (red), inconsistent from ANOVA processing (orange), rejected as an outlier (purple), or rejected as a duplicate (pink). Duplicates are measurements that have the same time stamp and RCS value, which occasionally occur. The middle subplot indicates the number of samples included in each monthly group. The colors within the bar graphs indicate the relative number of samples between the groups. The bottom subplot provides a boxplot of the distribution of the "accepted values" for each monthly group. The color of each boxplot indicates how alike that group is when compared to the other groups.
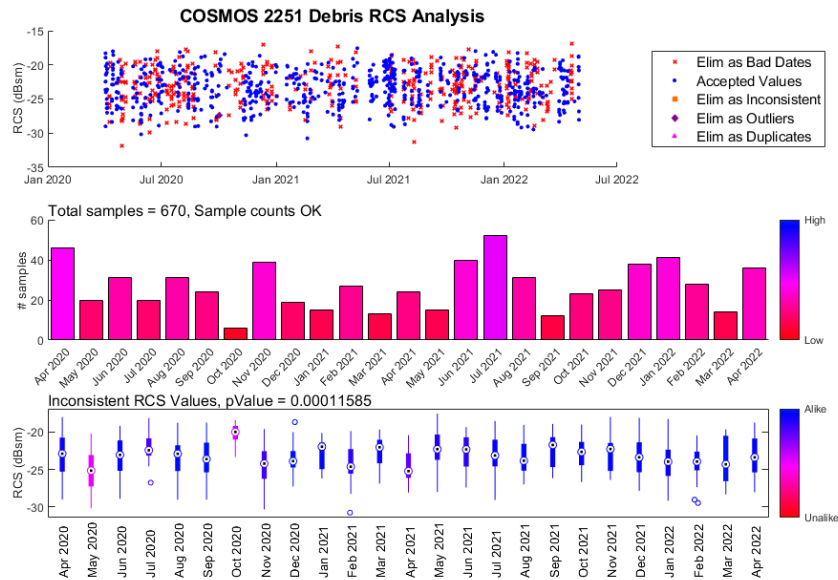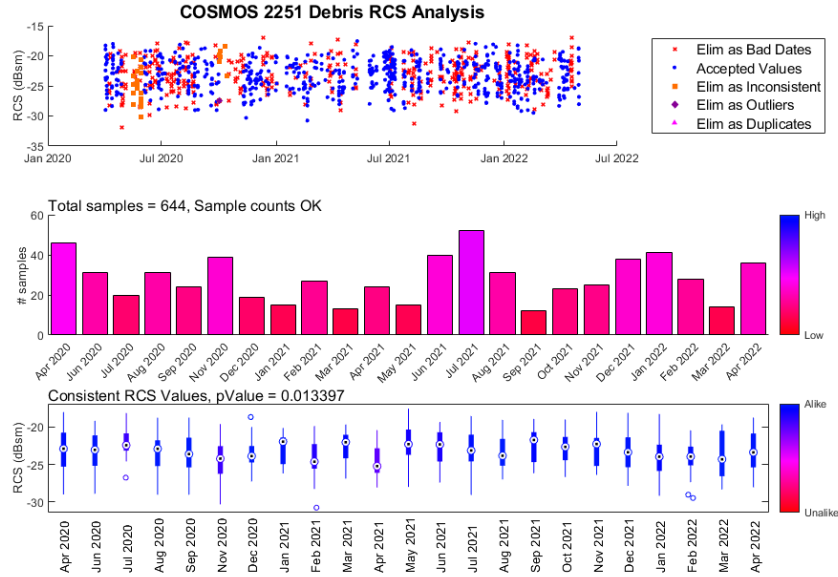

7

Figure 3. Consistency analysis for a piece of COSMOS 2251 debris after calibration sphere and ANOVA filtering

In this example, three iterations of ANOVA filtering were required in order to converge onto a statistically significant self-consistent set of RCS data. In the first iteration May 2020 was eliminated and then October 2020 in the second iteration. Finally, on the third iteration, the ANOVA *p-value* of ~0.013 exceeded the threshold of significance and the remaining groups of RCS values were considered consistent. Note that the middle and bottom subplots do not include monthly groups that have been eliminated as inconsistent in previous iterations. The remaining set of RCS measurements colored in blue in the top subplot of Figure 3 are considered the consistent set of RCS measurements which are then used for HBR and mass estimation.

HBR AND MASS ESTIMATION FROM RCS MEASUREMENTS

Once data filtering is complete, what remains is a well-conditioned set of RCS data which can be used for other applications, such as the estimation of unknown hard-body radii and masses. This section summarizes the methods CARA uses to estimate HBRs and masses for unknown objects using filtered RCS data as an input. A parallel study by Hall and Baars presents a full development of the equations and methods used below.[14] For brevity, this analysis includes only the most critical equations needed for obtaining HBR and mass estimates. Additionally, the results presented in this section use a subset of the SFK RCS data collected within a period two years prior from the study date of 2022-01-15.

Estimating the Statistically Expected Hard Body Radius of an Unknown Satellite

As a first step toward estimating unknown HBR values and uncertainty distributions, this analysis uses the NASA size estimation model to estimate RCS-based characteristic sizes. Applying Eq. (1) to the jth object produces a set of characteristic length estimates

$\{D_{j,n}, n=1\dots N_j^{RCS}\}$, which typically has considerable point-to-point variability or scatter. Sources of this scatter include the object's aspect-dependent radar reflection properties and projected area (which vary in time due to rotation and changing observational geometry), as well as RCS measurement noise. The mean characteristic length for the jth object is given by[14]

$$\overline{D}_j = \frac{1}{N_j^{RCS}} \sum_{n=1}^{N_j^{RCS}} D_{j,n} \tag{3}$$

The corresponding variance is

$$\sigma_{D_j}^2 = \frac{1}{N_j^{RCS}} \sum_{n=1}^{N_j^{RCS}} \left(D_{j,n} - \overline{D}_j\right)^2 \tag{4}$$

The derivation of these estimates assumes that the observed set $\{D_{j,n}, n=1\dots N_j^{RCS}\}$ provides an empirical representation of the uncertainty PDF of the object's characteristic length. Since the variable radar reflection properties of the object causes some of the variation of the $D_{j,n}$ values, this empirical PDF approximation tends to overestimate the variance of the object's actual characteristic size distribution.

If the SEM were free of any estimation inaccuracies and the RCS measurements were free of any measurement noise, then the relationship between the circumscribing HBR and the characteristic length for idealized spherical objects would be relatively simple: $R_j = D_j/2$. In order to quantify the bias and uncertainty for noisy measurements of non-spherical objects, Hall and Baars introduce an HBR estimation calibration factor, ϕ_j, into this relationship: $R_j = e^{\phi_j}(D_j/2)$.[14] Utilizing the *Database and Information System Characterizing Objects in Space* (DISCOS), the calibration factor is estimated by comparing known and RCS-based HBR estimates for a large set of "box" shaped objects with circumscribing HBRs less than or equal to 0.35 meters.[14,26,27] For the calibration data set examined, Hall and Baars determined a mean calibration factor of $\overline{\phi} = $ 0.306 and calibration standard deviation of $\sigma_\phi = $ 0.526.[14]

Putting all of these pieces together, the statistically expected HBR of the jth unknown satellite which accounts for uncertainties in both the characteristic size estimation and the HBR calibration process, is expressed analytically as

$$\overline{R}_j = \frac{\overline{D}_j I_1(\overline{\phi}, \sigma_\phi)}{2} \tag{5}$$

with the exponential expected value integral function given by

$$I_q(\overline{\phi}, \sigma_\phi) = e^{q\overline{\phi} + q^2\sigma_\phi^2/2} \tag{6}$$

The associated variance also has an analytical solution

$$\sigma_{R_j}^2 = \left[\frac{\left(\overline{D}_j^2 + \sigma_{D_j}^2\right) I_2(\overline{\phi}, \sigma_\phi)}{4}\right] - \overline{R}_j^2 \tag{7}$$

As mentioned earlier, using the empirical PDF approximation of Eq. (3) tends to result in $\sigma_{D_j}^2$ being overestimated, which in turn leads to an overestimated HBR variance $\sigma_{R_i}^2$.

Performance of RCS-based Hard-Body Radius Estimation

As a part of the Hall and Baars study, a set of 67,135 CARA conjunctions were analyzed to test the accuracy of the RCS-based HBR estimates.[14] These conjunctions comprised a set of known CARA primaries and known relatively small DISCOS secondaries (i.e. $R_2^K \le 0.35$ m) which had sufficient RCS data to allow HBR estimation. This set of "small-secondary" conjunctions provide a means of testing how well the RCS-based estimation method performs for secondary objects that are small enough to represent reasonable surrogates for the truly unknown secondary population.
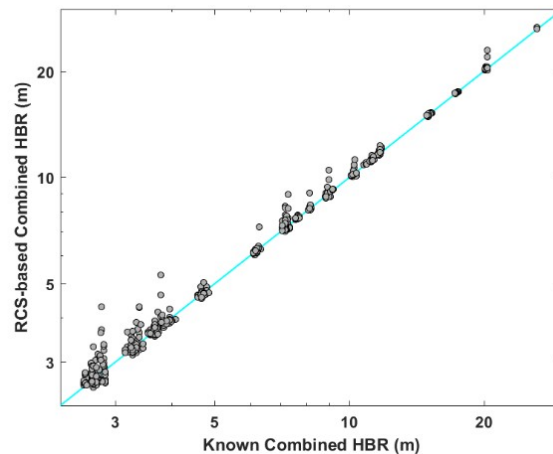

Figure 4. Combined hard-body radii for conjunctions involving small secondary objects

Analysis of secondary object sizes alone shows that the RCS-based estimation process generates HBR values that are accurate to within a rough factor of three in either direction. Figure 4 compares combined primary and secondary HBR values for small-secondary conjunctions by plotting $R_1^K + \overline{R}_2$ vs $R_1^K + R_2^K$. Despite the considerable uncertainties in estimating secondary object sizes, estimates for the combined HBR values for most known-on-unknown CARA conjunctions are not nearly as uncertain because CARA primary satellites typically have much larger HBR values than the selected secondary satellites.

An analysis 226,659 known-on-unknown CARA conjunctions that have sufficient auxiliary RCS data to allow secondary object size estimation has a lower 97.5% range of $\overline{R}_2 \le 0.36$ m. Notably, only 0.6% of the conjunctions have $\overline{R}_2 > ¿$ 1.5 m, the default HBR value currently used by the CARA system for unknown secondary objects.

Effective Hard-body Radius Collision Probability Approximation

Many methods exist to estimate the collision probability between tracked satellites, formulated using both semi-analytical approximations and MC techniques.[3-6] Most of these methods express the collision probability as a function of the combined HBR, i.e., $P_c = P_c(R)$, with the combined primary and secondary HBR, $R = R_1 + R_2$, treated as a known and constant value. For conjunctions

that involve unknown objects with uncertain RCS-based HBR estimates, the probability of collision can be approximated as $P_c = P_c(R_e)$, with the "effective" HBR given by[14]

$$R_e = \sqrt{(\overline{R}_1 + \overline{R}_2)^2 + \sigma_{R_1}^2 + \sigma_{R_2}^2} \tag{8}$$

where $\overline{R}_1$ and $\overline{R}_2$ are given by Eq. (5) for the primary and secondary satellites, respectively. Likewise, $\sigma_{R_1}^2$ and $\sigma_{R_2}^2$ are calculated from Eq. (7). When the primary object in the conjunction has known dimensions, the effective HBR reduces to

$$R_e = \sqrt{(R_1 + \overline{R}_2)^2 + \sigma_{R_2}^2} \tag{9}$$

where R_1 is the known HBR of the primary satellite. The probability of collision, $\overline{P}_c$, approximation for this type of conjunction is

$$\overline{P}_c \approx P_c\left(\sqrt{(R_1 + \overline{R}_2)^2 + \sigma_{R_2}^2}\right) \tag{10}$$

which accounts in an approximate manner for the magnitude and uncertainty of the RCS-based secondary HBR estimate.

Estimating the RCS- and OD-based Mass for LEO Objects Experiencing Atmospheric Drag

This analysis approximates the characteristic mass of a LEO satellite that experiences measurable levels of atmospheric drag using the expression[28]

$$M_j = A_j B_j C_j \approx (\pi D_j^2/4) B_j C_j \tag{11}$$

In this expression, M_j indicates the mass that characterizes the atmospheric drag experienced by the jth satellite, which is proportional to the projected area, A_j, the inverse ballistic coefficient, B_j, and the drag coefficient, C_j. Notably, this expression uses the RCS-based characteristic length to estimate the cross-sectional area of the satellite projected onto the plane normal to the local atmospheric flow, $A_j \approx (\pi D_j^2/4)$, which is a rough approximation, especially for highly elongated or flattened objects. Accounting for the uncertainty in the characteristic length the mean projected area is

$$\overline{A}_j = \frac{\pi (\overline{D}_j^2 + \sigma_{D_j}^2)}{4} \tag{12}$$

The corresponding variance is

$$\sigma_{A_j}^2 = \left(\frac{\pi^2}{16 N_j^{RCS}} \sum_{n=1}^{N_j^{RCS}} D_{j,n}^4\right) - \overline{A}_j^2 \tag{13}$$

The mean and variance of the inverse ballistic coefficient, $\overline{B}_j$ and $\sigma_{B_j}^2$, respectively, are estimated empirically by combining a series of OD solutions accumulated over the six months prior to the calibration epoch date. Specifically, the analysis uses a series of Vector Covariance Messages (VCMs) separated by one week or more in time that each represent an OD solution for the jth satellite. The corresponding ballistic coefficients, ¿, typically number $N_j^{VCM} \approx 25$ for most

satellites. The ballistic coefficients, $\beta_{j,m}$, and associated 1-sigma OD estimation uncertainties, $\Delta\beta_{j,m}$, are then combined using a weighted averaging scheme. The first step in the process is to calculate the inverse ballistic coefficient and uncertainty for the mth VCM available for the jth satellite

$$B_{j,m}=1/\beta_{j,m} \wedge \Delta B_{j,m}=\Delta\beta_{j,m}/\beta_{j,m}^2 \tag{14}$$

The next step calculates the weighted average

$$\overline{B}_j=\frac{1}{W_j}\sum_{m=1}^{N_j^{VCM}}W_{j,m}B_{j,m} \tag{15}$$

with $W_{j,m}=(\Delta B_{j,m})^{-2}$ and $W_j=\sum_m W_{j,m}$ The analysis estimates the associated variance using a hybrid scheme as follows

$$\sigma_{B_j}^2=max\left(W_j^{-1},V_j\right) with\, V_j=W_j^{-1}\left[\frac{N_j^{VCM}}{N_j^{VCM}-1}\sum_{m=1}^{N_j^{VCM}}W_{j,m}\left(B_{j,m}-\overline{B}_j\right)^2\right]^{1/2} \tag{16}$$

which conservatively uses the larger of the variances estimated using two methods: the first assumes statistical independence of the $B_{j,m}$ values, yielding a variance equal to W_j^{-1}; the second accounts for the observed scatter of the $B_{j,m}$ values, yielding the empirical estimate of variance V_j.[29]

This study bounds the drag coefficient to $C_{min}=¿$ 2.1 and $C_{max}=¿$ 2.9, based on the range of drag coefficients presented in previous analyses.[28,30] The uniform PDF approximation yields a mean of $\overline{C}_j=(C¿¿max+C_{min})/2=¿¿$ 2.5, and variance $\sigma_{C_j}^2=(C¿¿max-C_{min})^2/12=¿¿$ 0.053.

Much like before, utilizing comparisons against the DISCOS database, Hall and Baars introduced a mean calibration factor of $\overline{\psi}=¿$ -0.173 and calibration standard deviation of $\sigma_\psi=¿$ 0.971.[14] The estimate for σ_ψ indicates significant satellite-to-satellite variation.

The statistically expected mass of the jth unknown satellite must account for uncertainties both in the mass estimation process and the mass calibration process, which results in a 4-D expectation value integral that has an analytical solution

$$\overline{M}_j\approx I_1\left(\overline{\psi},\sigma_\psi\right)\left[\overline{A}_j\overline{B}_j\overline{C}_j\right] \tag{17}$$

This expected value averages over a set of four random variables $\{D_j,\psi_j,B_j,C_j\}$, and accounts in an approximate way for the combined uncertainties of these quantities. The associated variance also has an analytical solution

$$\sigma_{M_j}^2=I_2\left(\overline{\psi},\sigma_\psi\right)\left[\left(\overline{A}_j^2+\sigma_{A_j}^2\right)\left(\overline{B}_j^2+\sigma_{B_j}^2\right)\left(\overline{C}_j^2+\sigma_{C_j}^2\right)\right]-\overline{M}_j^2 \tag{18}$$

Performance of RCS- and OD-based Mass Estimation

The mass calibration process used a set of 541 box-shaped objects from the DISCOS database for which there was sufficient RCS data and VCM inputs to perform a mass estimation. Figure 5 depicts the plots the calibrated mass estimates on the vertical axis vs the known masses on the horizontal axis. This figure illustrates the significant level of uncertainty associated with the mass calibration process. The calibration uncertainties limit the accuracy of mass estimation process to within a factor of four (for potential mass overestimations) to ten (for potential mass underestimations).
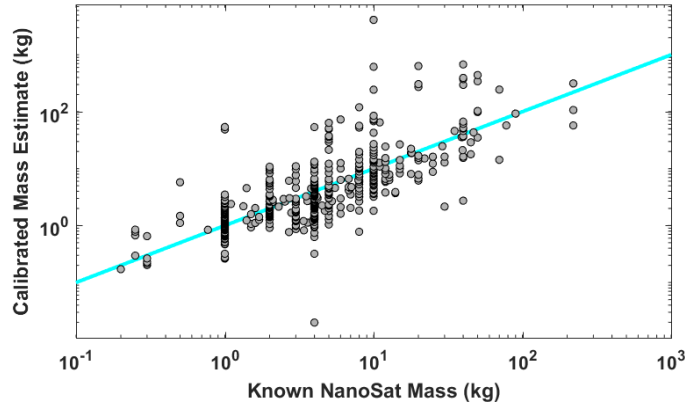

Figure 5. Comparison of calibrated vs known satellite mass values

Estimating LEO satellite masses requires several assumptions and approximations:

1. The mass estimation method assumes that correlations known to exist between A_j, B_j, and C_j can be neglected.
2. The method roughly approximates atmospheric drag projected areas as $A_j \approx \left(\pi\, D_j^2 / 4 \right)$.
3. The method assumes a log-normal distribution for the inverse ballistic coefficient uncertainty PDF, based on empirically-determined means and variances.
4. The method assumes a uniform distribution for the drag coefficient PDF.

The combined effects of these assumptions and approximations significantly limits the accuracy of the mass calibration and estimation process.

CONCLUSION

The methods formulated in this study to filter Space Fence RCS data provide a well-conditioned set of RCS measurements appropriate for HBR and mass estimation, among other applications. A critical first step involves the elimination of RCS measurements from days where the Space Fence sensor has provided measurements which exceed a 1.5 dBsm departure from calibration sphere reference values. Using multiple radar calibration spheres to identify such days helps ensure that the filtering process can perform even when the Space Fence reports limited tracking on one or more calibration spheres.

The ANOVA filtering process adds a secondary set of filters in order to ensure that RCS measurements are consistent over time. This filter removes spurious measurement biases yet maintains the noise inherent in RCS measurements. It is expected that an irregularly shaped

tumbling object such as a piece of debris could produce a wide range of RCS values, therefore it is not necessarily desirable to remove measurement noise from these data. Caution should be employed when setting the *p-value* threshold to stop the ANOVA filtering process since the filter can be aggressive in eliminating inconsistent data when the threshold is set too high.

Using the filtered RCS data and the NASA SEM model, a distribution of characteristic lengths can be generated for each object. A mean expected HBR and variance can then be estimated which accounts for uncertainties in the RCS data. Analysis of the size calibration process indicates that RCS-based HBR estimates are accurate to within a rough factor of three. Taken as an ensemble, an estimated 97.5% of unknown secondary objects involved in CARA conjunctions have statistically expected HBRs estimated below 36 cm, and less than 0.6% exceed 1.5 m.

For conjunctions that involve unknown objects with RCS-based HBR estimates, the statistically expected probability of collision can be approximated using the expression $\overline{P}_c \approx P_c(R_e)$. The "effective" combined HBR, R_e, given by Eqs. (8) or (9), accounts in an approximate manner for both the magnitude and uncertainty of the RCS-based size estimates.

The mass calibration analysis indicates that RCS- and OD-based mean mass estimates are accurate to within a factor four to ten, roughly. This relatively large mass estimation uncertainty is due in part to the fact that the analysis uses several rough approximations, such as neglecting correlations known to exist between ballistic coefficients and projected areas, as well as assuming approximate forms for the PDFs of the ballistic and drag coefficients.

ACKNOWLEDGMENTS

NOTATION

A_j the cross-sectional area projected by the jth satellite

$\overline{A}_j$ the mean cross-sectional area projected by the jth satellite

$B_{j,m}$ the inverse ballistic coefficient for the mth VCM available for the jth satellite

$\overline{B}_j$ the weighted average inverse ballistic coefficient of the jth satellite

$\overline{C}_j$ the mean aerodynamic drag coefficient of the jth satellite

C_{min} the minimum drag coefficient used in the study

C_{max} the maximum drag coefficient used in the study

D_j the characteristic length estimated for the jth satellite

$\overline{D}_j$ the mean characteristic length estimated for the jth satellite

$D_{j,n}$ the characteristic object size indicated by the nth RCS measurement available for the jth satellite

$g_{SEM}(z)$ the interpolation function for the RCS-based characteristic size estimate

$I_q(\overline{x}, \sigma_x)$	the exponential expected value integral function
M_j	the mass that characterizes the atmospheric drag experienced by the jth satellite
$\overline{M}_j$	the statistically expected mass for the jth satellite
N_j^{RCS}	the number of RCS measurements available for the jth satellite
N_j^{VCM}	the number of VCMs available for the jth satellite
P_c	the collision probability for a conjunction between two satellites
$\overline{P}_c$	the statistically expected collision probability
$P_c(R)$	the collision probability expressed as a function of the combined HBR
R_e	the effective HBR of a conjunction
R_j	the circumscribing hard-body radius for the jth satellite
$\overline{R}_j$	the statistically expected HBR for the jth satellite
RCS_{dBsm}	the radar cross-section measured in decibels relative to one square meter
RCS_{m^2}	the radar cross-section measured in units of square meters
$U(x)$	the unit step function for the jth satellite
V_j	the empirical estimate of variance
W_j	the combined inverse ballistic coefficient weights for the jth satellite
$W_{j,m}$	the inverse ballistic coefficient weight for the mth VCM available for the jth satellite
$Y_{j,n}$	the radar cross section in units of m² for the nth RCS measurement available for the jth satellite
z	the dimensionless RCS value
$\beta_{j,m}$	the ballistic coefficient of the mth VCM available for the jth satellite
$\Delta B_{j,m}$	the inverse uncertainty of the mth VCM available for the jth satellite
$\Delta \beta_{j,m}$	the 1-sigma OD estimation uncertainty of the mth VCM available for the jth satellite
$\lambda_{j,n}$	the radar wavelength for the nth RCS measurement available for the jth satellite
ϕ_j	the logarithmic HBR calibration factor for the jth satellite
$\overline{\phi}$	the mean logarithmic HBR calibration factor estimated from a set of calibration satellites
$\overline{\psi}$	the mean logarithmic mass calibration factor estimated from a set of calibration satellites

$\sigma^2_{A_j}$ the variance of the cross-sectional area projected by the jth satellite

$\sigma^2_{D_j}$ the variance of the characteristic length of the jth satellite

$\sigma^2_{C_j}$ the variance of the drag coefficient for the jth satellite

$\sigma^2_{M_j}$ the variance of the statistically expected mass for the jth satellite

$\sigma^2_{R_j}$ the variance of the statistically expected HBR for the jth satellite

σ_{ϕ} the logarithmic HBR calibration standard deviation from a set of calibration satellites

σ_{ψ} the logarithmic mass calibration standard deviation from a set of calibration satellites

[1] L.K. Newman and M.D. Hejduk, "NASA Conjunction Assessment Organizational Approach and the Associated Determination of Screening Volume Sizes," *International CA Risk Assessment Workshop*, 19-20 May 2015.

[2] B.D. Tapley, B.E. Schutz, and G.H. Born, *Statistical Orbit Determination*, Elsevier Academic Press, Burlington, MA, 2004.

[3] J.L. Foster and H.S. Estes, "A Parametric Analysis of Orbital Debris Collision Probability and Maneuver Rate for Space Vehicles," NASA/JSC-25898, Aug. 1992.

[4] K. Chan, *Spacecraft Collision Probability*, El Segundo, CA, The AeroSpace Corporation, 2008.

[5] S. Alfano, "Satellite Conjunction Monte Carlo Analysis," *AAS SpaceFlight Mechanics Meeting*, Pittsburgh, PA, Paper 09-233, Feb. 2009.

[6] L. Baars, D. Hall, and S. Casali, "Assessing GEO and LEO Repeating Conjunctions Using High Fidelity Brute Force Monte Carlo Simulations," *AAS/AIAA Astrodynamics Specialist Conference*, Portland, ME, Paper 19-612, Aug. 2019.

[7] M. Hejduk, "Space Catalogue Size Profiling for HBR," *Flight Dynamics Support Services Technical Orders*, FDSS-TO #-0001, a.i. solutions, Inc., Aug. 2014.

[8] A.C. Boley and M. Byers, "Satellite mega-constellations create risks in Low Earth Orbit, the atmosphere and on Earth," *Scientific Reports*, Article 10642, May 2021.

[9] S. Thiele and A. Boley, "Investigating the risks of debris-generating ASAT tests in the presence of megaconstellations," *AMOS Conference Proceedings*, 2021.

[10] D. Barton, "Final Report of the Haystack Orbital Debris Data Review Panel," NASA Technical Memorandum 4809, Feb. 1998.

[11] E. Doyle, "Space Fence Ground-Based Radar System Increment 1 Selected Acquisition Report," *Defense Acquisition Management Information Retrieval*, DD-A&T(Q&A)832-438, Dec. 2019.

[12] S. Erwin, "Space Fence surveillance radar site declared operational," https://spacenews.com/space-fence-surveillance-radar-site-declared-operational/, *Space News*, 28 Mar 2020, Retrieved 26 May 2022.

[13] C.L. Stokely, J.L. Foster, E.G. Stanbery, J.R. Benbrook, and Q. Juarez, "Haystack and HAX Radar Measurements of the Orbital Debris Environment," *National Aeronautics and Space Administration Report*, Orbital Debris Program Office, JSC-62815, Nov. 2006.

[14] D.T. Hall and L.G. Baars, "Collision and Fragmentation Probabilities for Satellites with Size and Mass Estimates Based on Radar Observations," in preparation, April 2022.

[15] M.D. Hejduk and D. DePalma, "Comprehensive Radar Cross-Section 'Target Typing' Investigation for Spacecraft," Astorum Consulting LLC, 2010.

[16] P. Mishra, U. Singh, C.M. Pandey, P. Mishra, and G. Pandey, "Application of Student's *t*-test, Analysis of Variance, and Covariance," *Annals of Cardiac Anaesthesia*, Volume 22, Issue 4, Oct.-Dec. 2019.

[17] J.H. McDonald, "Handbook of Biological Statistics, 3rd edition," *Sparky House Publishing*, 2014.

[18] "NIST/SEMATECH e-Handbook of Statistical Methods," http://www.itl.nist.gov/div898/handbook/, Retrieved May 2022.

[19] B. Iglewicz and D. Hoaglin, "Volume 16: How to Detect and Handle Outliers," *The ASQC Basic References in Quality Control: Statistical Techniques*, 1993.

[20] "MATLAB Function Reference," MathWorks, 2022.

[21] G.W. Snedecor and W.G. Cochran, *Statistical Methods*, Iowa State University Press, 8th ed., 1989.

[22] H. Levene, *Contributions to Probability and Statistics: Essays in Honor of Harold Hotelling*, Stanford University Press, 1960.

[23] J.W. Tukey, "Comparing Individual Means in the Analysis of Variance," *Biometrics*, Vol 5., No. 2, Jun. 1949.

[24] G.D. Ruxton and G. Beauchamp, "Time for some a priori thinking about post hoc testing," *Behavioral Ecology*, Feb. 2008.

[25] L.E. Toothaker, "Multiple Comparison Procedures," *Quantitative Applications in the Social Sciences*, Vol. 89, Oct. 1992.

[26] T. Flohrer, S. Lemmens, B. Bastida Virgili, H. Krag, H. Klinkrad, E. Parrilla, N. Sanchez, J. Oliveira, F. Pina, "DISCOS – Current Status and Future Developments," Proc. 6th European Conference on Space Debris, ESA SP-723, Darmstadt, Germany, Apr. 2013.

[27] F. Mclean, S. Lemmens, Q. Funke, and V. Braun, "DISCOS 3: An Improved Model for ESA's Database and Information System Characterising Objects in Space," Proc. 7th European Conference on Space Debris, Darmstadt, Germany, Jun. 2017.

[28] T. Lechtenberg, "An Operational Algorithm for Evaluating Satellite Collision Consequence," *AAS Astrodynamics Specialist Conference*, Portland, ME, Paper AAS 19-669, 2019.

[29] D.F. Gatz and L. Smith, "The standard error of a weighted mean concentration-I. Bootstrapping vs other methods," *Atmospheric Environment*, Vol. 29, No. 11, pp. 1185-1193, Jun. 1995.

[30] T. Lechtenberg and M.D. Hejduk, "Assessment and Validation of Collision "Consequence" Method of Assessing Orbital Regime Risk Posed by Potential Satellite Conjunctions," *Hypervelocity Impact Symposium*, Destin, FL, Paper HVIS2019-061, 2019.